AGU PUBLICATIONS

JGR

Journal of Geophysical Research: Atmospheres

RESEARCH ARTICLE

10.1002/2015JD023844

Key Points:
- Consistent amount effect is not observed in storms
- Deuterium excess correlated with variables related to convective activity
- Rain to vapor isotope ratios indicate rain evaporation and distinct upper level vapor sources

Supporting Information:
- Supporting Information S1
- Data Set S1

Correspondence to:
J. L. Conroy,
jconro@illinois.edu

Citation:
Conroy, J. L., D. Noone, K. M. Cobb, J. W. Moerman, and B. L. Konecky (2016), Paired stable isotopologues in precipitation and vapor: A case study of the amount effect within western tropical Pacific storms, *J. Geophys. Res. Atmos.*, *121*, 3290–3303, doi:10.1002/2015JD023844.

Received 24 JUN 2015
Accepted 20 MAR 2016
Accepted article online 25 MAR 2016
Published online 8 APR 2016

Paired stable isotopologues in precipitation and vapor: A case study of the amount effect within western tropical Pacific storms

Jessica L. Conroy[1,2], David Noone[3,4,5], Kim M. Cobb[6], Jessica W. Moerman[6], and Bronwen L. Konecky[3,4]

[1]Department of Geology, University of Illinois at Urbana-Champaign, Champaign, Illinois, USA, [2]Department of Plant Biology, University of Illinois at Urbana-Champaign, Urbana, Illinois, USA, [3]College of Earth, Ocean, and Atmospheric Sciences, Oregon State University, Corvallis, Oregon, USA, [4]Cooperative Institute for Research in Environmental Sciences, University of Colorado Boulder, Boulder, Colorado, USA, [5]Department of Atmospheric and Oceanic Sciences, University of Colorado Boulder, Boulder, Colorado, USA, [6]School of Earth and Atmospheric Sciences, Georgia Institute of Technology, Atlanta, Georgia, USA

Abstract Understanding controls on the stable isotopic composition of precipitation and vapor in the West Pacific Warm Pool is vital for accurate representation of convective processes in models and correct interpretation of isotope-based paleoclimate proxies, yet a lack of direct observational evidence precludes the utility of these isotopic tracers. Results from a measurement campaign at Manus Island, Papua New Guinea from 28 April to 8 May 2013 demonstrate variability in the stable isotopic composition (δD and δ^{18}O) of precipitation and vapor in individual precipitation events and over a 10 day period. Isotope ratios in water vapor and precipitation progressively increased throughout the period of measurement, coincident with a transition from high to low regional convective activity. Vapor isotope ratios approached equilibrium with seawater during the quiescent period and likely reflected downwind advection of distilled vapor and re-evaporation of rainfall during the period of regional convection. On a 5 min timescale across individual storms, isotope ratios in precipitation were strongly correlated with isotope ratios in surface vapor. However, individual precipitation isotope ratios were not strongly correlated with surface meteorological data, including precipitation rate, in all storms. Yet across all events, precipitation deuterium excess was negatively correlated with surface temperature, sea level pressure, and cloud base height and positively correlated with precipitation rate and relative humidity. Paired surface precipitation and vapor isotope ratios indicate condensation at boundary layer temperatures. The ratio of these paired values decreased with increasing precipitation rate during some precipitation events, suggesting rain re-evaporation and precipitation in equilibrium with an isotopically distinct upper level moisture source. Results from the short campaign support the interpretation that isotope ratios in precipitation and vapor in the western tropical Pacific are indicators of regional convective intensity at the timescale of days to weeks. However, a nonstationary relationship between rain rate and stable isotope ratios in precipitation during individual convective events suggests that condensation, rain evaporation, moisture recycling, and regional moisture convergence do not always yield an amount effect relationship on intraevent timescales.

1. Introduction

The isotopic amount effect, whereby higher precipitation rates are associated with lower isotope ratios, is recognized as the most salient feature of monthly, seasonal, and annual isotopic variability in tropical precipitation [*Dansgaard*, 1964; *Rozanski et al.*, 1993; *Araguas-Araguas et al.*, 2000] and has been observed at weekly [*Moerman et al.*, 2013] and simulated at subweekly (4 day) timescales [*Risi et al.*, 2008]. However, the amount effect is not consistently expressed on event timescales [*Miyake et al.*, 1968; *Vimeux et al.*, 2005; *Risi et al.*, 2008; *Moerman et al.*, 2013; *Kurita*, 2013], an observation that points to diverse controls on the stable isotopic composition of tropical precipitation. Although long thought to be a result of a condensation mechanism [e.g., *Dansgaard*, 1964; *Vuille et al.*, 2003], recent studies using both models and observations have hypothesized that the amount effect could be a result of other processes, including downdraft moisture recycling [*Risi et al.*, 2008], large-scale organized convection and associated stratiform rain [*Kurita*, 2013], regional circulation, shifting moisture source regions and downwind transport of isotopically depleted vapor [*Lawrence et al.*, 2004; *Kurita et al.*, 2009], or a decrease in the relative amount of surface vapor versus converged vapor, conceptualized as the ratio of surface evaporation to precipitation [*Lee et al.*, 2007; *Moore et al.*, 2014]. Adding to the complexity, the potential mechanisms that determine the empirical relationship between the stable isotopic composition of precipitation and precipitation amount may vary over space and time [*Moerman et al.*, 2013]. Thus, we require data sets of stable isotope ratios in precipitation across a range of timescales from a diversity of sites in order to constrain the possible mechanisms behind the amount effect.

High-frequency measurements of isotope ratios in precipitation through individual convective events are useful for identifying specific convective processes and have provided constraints on isotopic exchange between vapor and precipitation, precipitation height, the role of advection, and intraseasonal oscillations [*Miyake et al.*, 1968; *Coplen et al.*, 2008; *Yoshimura et al.*, 2010; *Kurita et al.*, 2011]. Coupled $\delta^{18}O$ and δD measurements (defined as the isotopic ratios $^{18}O/^{16}O$ and $^{2}H/^{1}H$, expressed in ‰ deviation from the Vienna Standard Mean Ocean Water (VSMOW), respectively) from vapor and precipitation through individual storms, which are becoming more common with the advent of field-deployable cavity ring down spectroscopy [*Tremoy et al.*, 2012; *Kurita*, 2013], can provide even more insights into the microphysical processes that define convection. At the event scale, the offset between equilibrium fractionation and the observed ratio of paired surface vapor to precipitation isotope ratios ($R_{precipitation}/R_{vapor}$, where R is the ratio of heavy to light isotopes) describes an effective fractionation and can also aid in inferring conditions during condensation [*Noone*, 2012; *Bailey et al.*, 2013, 2015b]. Deuterium excess ($dxs = \delta D - 8\delta^{18}O$ [*Dansgaard,* 1964]) values similarly give insight into the role of kinetic fractionation [*Blossey et al.*, 2010; *Bolot et al.*, 2013].

Here we present δD, $\delta^{18}O$, $R_{precipitation}/R_{vapor}$, and dxs data from paired, intraevent vapor and precipitation stable isotope measurements taken on Manus Island, Papua New Guinea. Manus, a small island in the heart of the West Pacific Warm Pool—the world's largest zone of deep convection [*Chiang*, 2009]—is ideally situated to investigate convective processes. In the West Pacific Warm Pool, large changes in the stable isotopic composition of precipitation and vapor are associated with the Madden Julian Oscillation [*Kurita et al.*, 2011; *Berkelhammer et al.*, 2012; *Moerman et al.*, 2013], the dominant mode of tropical precipitation at 30–90 day timescales [*Madden and Julian*, 1971]. As the Madden Julian Oscillation (MJO) strongly influences Manus precipitation amount and the degree of convective organization [*Deng et al.*, 2013], Manus is an ideal location to investigate high temporal resolution variability in the stable isotopic composition of vapor and precipitation. In the subsequent sections, we describe the stable isotope data and assess their relationship to key atmospheric variables. We then evaluate the isotopic signatures of convective processes in both vapor and precipitation and investigate potential amount effect-related mechanisms at Manus on intraevent (~1 km; hours) to synoptic scales (~1000 km; days to weeks).

2. Study Site and Methodology

The stable isotopic composition of water vapor, precipitation, and seawater was measured from 28 April to 8 May 2013 at the United States Department of Energy Atmospheric Radiation Measurement (ARM) facility located at Momote airport on Manus Island, Papua New Guinea (Figure 1). The highly instrumented Manus ARM site (2°3′40″S, 147°25′32″E, 4 m above sea level) sits in an open plain 340 m away from the ocean and is minimally impacted by terrestrial influences, such as soil evaporation or transpiration [*Riihimaki and Long*, 2014]. To provide context for the new observations of the stable isotope ratios of precipitation at Manus, Figure 1 shows mean April–May precipitation δD values simulated by an isotope-enabled climate model, which range from −30 to −45‰ around and to the north of Manus, surrounding a region where precipitation rates are high [*Yoshimura et al.,* 2008]. South of New Guinea, higher April–May mean precipitation δD values coincide with lower precipitation rates.

Isotopic ratios of water vapor were measured at the Manus ARM facility on a Picarro L1102-*i* water isotope analyzer installed in a climate-controlled shed at the site. Copper tubing (6.35 mm outer diameter), heated with self-regulating heat tape, drew ambient air from a height of 2.54 m into the instrument at a rate of 1 L/min. The fast speed of the pump and the short length of the inlet tubing preclude a strong memory effect due to differences in the adherence of the different isotopologues of water to the walls of the tubing. Resulting data were calibrated with National Institute of Standards and Technology (NIST)-VSMOW, NIST-GISP (Greenland Ice Sheet Precipitation), and NIST-SLAP (Standard Light Antarctic Precipitation) waters as well as three internal lab water standards ($\delta^{18}O = -16.4$, −4.6, 5.5‰, δD −98.9‰, −25.6‰, 4.0‰) at the beginning and end of the measurement period via manual injections with a syringe pump. Assessment of instrument drift was conducted with periodic measurement of vapor from a bubbler [*Bailey et al.*, 2015a], similar in protocol and design to the system described in *Steen-Larsen et al.* [2013], *Ellehoj et al.* [2013], and *Steen-Larsen et al.* [2014]. In this setup, water of

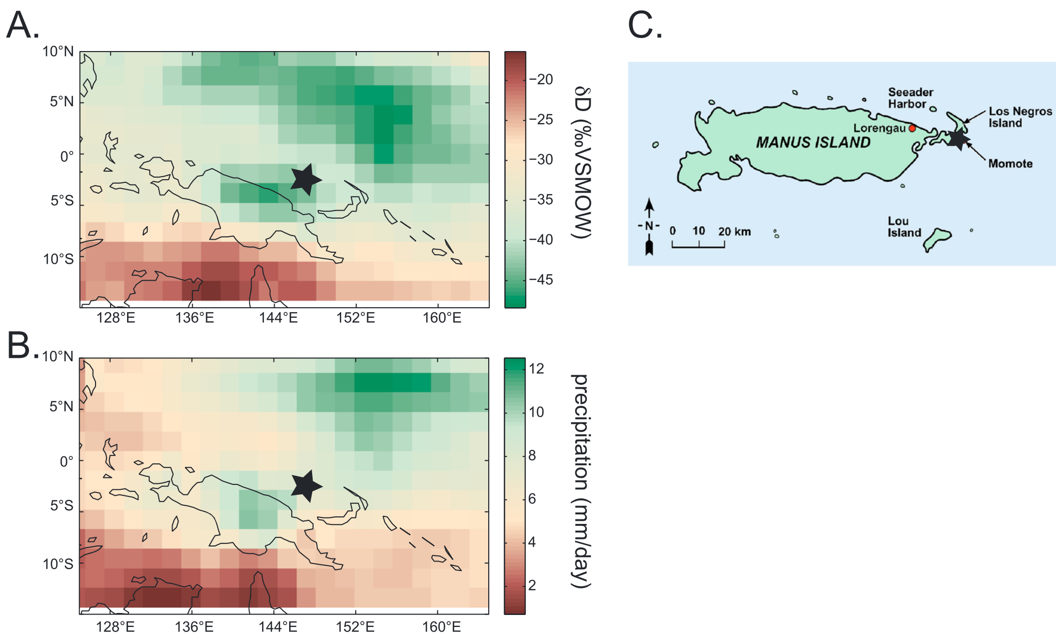

Figure 1. (a) Mean April–May δD value of precipitation for region taken from isoGSM nudged simulation, 1980–2008 [*Yoshimura et al.*, 2008]. (b) Mean April–May precipitation for region from isoGSM nudged simulation, 1980–2008 [*Yoshimura et al.*, 2008]. Star indicates location of Manus Island. (c) Map of Manus Island (courtesy of ARM), star showing location of ARM facility on Los Negros Island.

known isotopic value ($\delta^{18}O = -9.0‰$, $\delta D = -60.7‰$) was held at a near-constant temperature (26.0–30.0°C) in an insulated glass vessel. Saturated air from the vessel was mixed with a stream of ambient air passed through a vessel containing Drierite, in order to control water vapor concentration and prevent possible condensation in the tubing, and then drawn into the Picarro as the reference standard. Drift was minimal during the measurement period and can be accounted for by the varying temperature precision (Table S1). The humidity-isotope response of this instrument was calculated during the campaign using repeated injections of water of a known isotopic value ($\delta^{18}O = -16.4$, 5.5‰, δD −98.9‰, 4.0‰) at varying volumes. Instrument uncertainty exceeds the concentration bias [*Johnson et al.*, 2011; *Samuels-Crow et al.*, 2014; *Bailey et al.*, 2015a] for this instrument at water vapor concentrations above 25,000 ppmv (Figure S1). Measured water vapor concentration was consistently greater than 25,000 ppmv, so we did not correct for varying vapor concentration through time.

Here we report the δD and $\delta^{18}O$ values of measured near-surface vapor (henceforth δD_v, $\delta^{18}O_v$) in 5 min averaged intervals. Precision is ±0.1‰ (1 SE) for $\delta^{18}O_v$ and ±0.3‰ (1 SE) for δD_v, based on the average standard deviation of 20 s measurements within 5 min intervals. Vapor deuterium excess precision is ±1.2‰ (1 SE) based on δD_v and $\delta^{18}O_v$ precision and assuming uncorrelated error. Accuracy, as measured by comparison of measured and calibrated internal standard values listed above, is ±0.1‰ for $\delta^{18}O_v$ and ±0.8‰ for δD_v. We primarily discuss vapor isotopic variability in δD_v, as the ratio of precision to the overall standard error of 5 min averaged data is lower for δD (0.02) relative to $\delta^{18}O$ (0.08).

A total of 159 precipitation samples were collected at discrete intervals throughout seven rain events, six of which produced at least three samples. All samples were immediately sealed in 3.5 mL crimp top glass vials and refrigerated in the dark until analysis. Ninety-six samples were collected manually using a polypropylene separatory funnel connected to a 13 cm funnel or plastic bucket, and the remaining 65 were collected using a robotic rain water sampler. The robotic collector is similar in design to the collector described by [*Coplen et al.*, 2008] with modifications to collect and internally seal samples in 20 mL vials, minimizing evaporation, based on either duration (5 min) or liquid volume (20 mL), depending on the measured rain rate. Twenty-three seawater samples were taken from coastal locations around the island (Data Set S1) and promptly sealed in 3.5 mL crimp top vials.

Precipitation and seawater samples were measured on a Picarro L2120-*i* water isotope analyzer at the University of Illinois Urbana-Champaign. Reported data were calibrated with NIST-VSMOW, NIST-GISP, and NIST-SLAP and three internal lab standards ($\delta^{18}O = -10.2$, −6.8, 0.3‰, δD −72.3‰, −41.9‰, 0.9‰). Cross-instrument calibration with

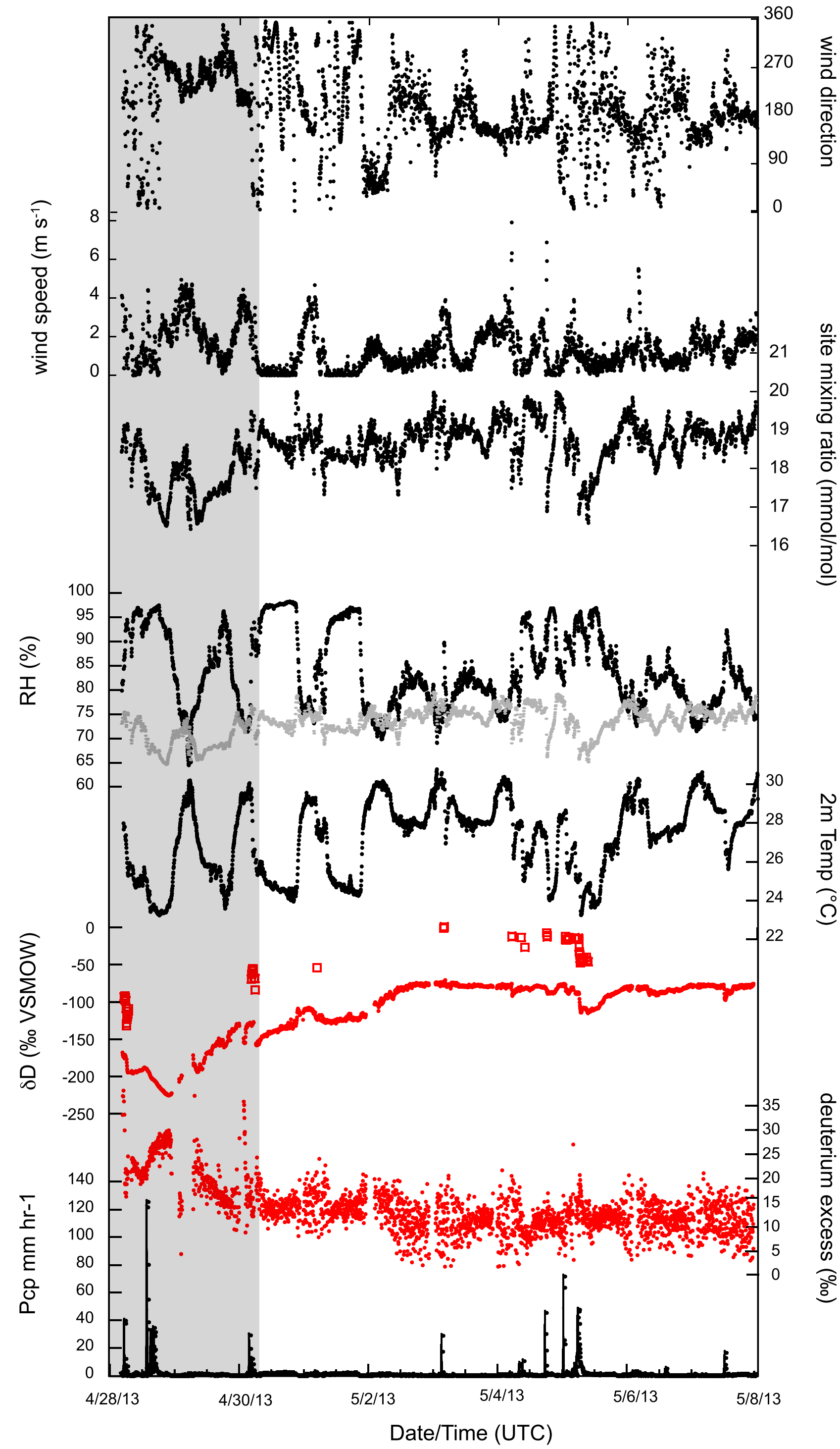

Figure 2. The 5 min averaged (from top to bottom) Manus wind direction, wind speed, mixing ratio, relative humidity, temperature, δD_v (red circles) and δD_p (red squares), vapor deuterium excess, and precipitation rate. Gray relative humidity curve denotes relative humidity with respect to mean daily AVHRR SST of 29.6°C near the site over the course of the investigation. Gray shaded time period denotes period of overall lower δD_v and δD_p, and westerly winds.

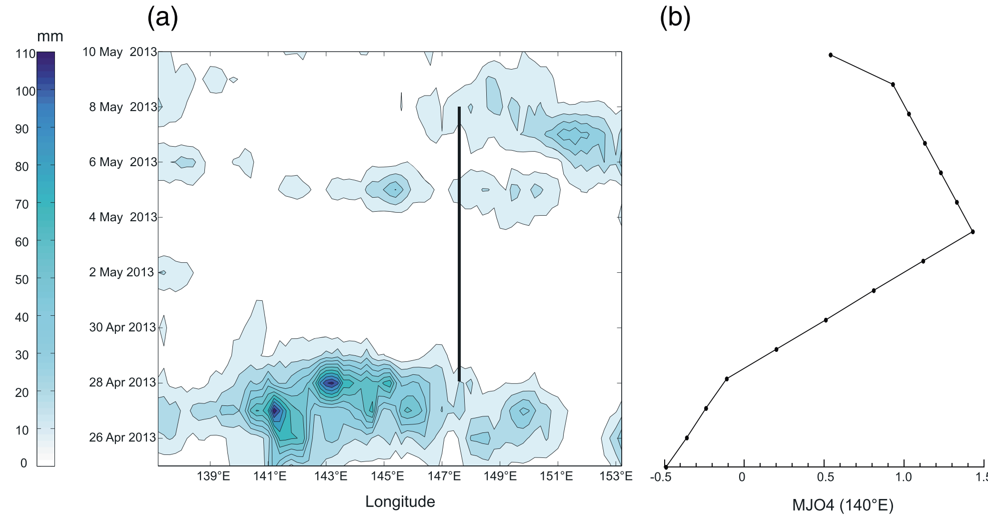

Figure 3. (a) Hovmöller plot of daily 3B42 TRMM precipitation (mm/d) averaged from 3°S to 1°S [*Kummerow et al.*, 1998]. Bold line indicates longitude of Manus (147.5°E) and period of measurement campaign. (b) MJO 4 Index (140°E). Negative values indicate enhanced convection; positive values indicate suppressed convection.

internal lab standards indicates no instrument-specific isotopic offsets in the calibrated results. Total measurement error was determined from analyses of known liquid standards and found to be <0.1‰ for $\delta^{18}O$ and 0.8‰ for δD values. Memory and drift corrections were applied using the internal standards listed above [*van Geldern and Barth*, 2012]. Isotopic data are interpolated into 5 min intervals for assessment against 5 min averaged vapor values; raw data are provided in Data Set S3. We also assessed the precipitation memory coefficient using two internal lab standards ($\delta^{18}O = -10.2, -6.8$, δD -72.3‰, -41.9‰) to determine how a previous precipitation sample could influence the isotopic composition of the subsequent sample, as we were unable to dry the interior of the separatory funnel in between the rapid intraevent measurements. After flushing and draining the separatory funnel with 10 mL of one standard, making sure to coat the interior of the funnel, we passed 5 mL of the second standard through the setup. 5 mL represents the smallest sample collected, and thus, a maximum memory effect. We calculate memory coefficients of 9.20×10^{-1} for $\delta^{18}O$ and 9.45×10^{-1} for δD [*Van Geldern and Barth*, 2012, equation 2]. Applying these coefficients to the measured intraevent precipitation $\delta^{18}O$ and δD values resulted in mean offsets of 0.03 ± 0.04‰ for $\delta^{18}O$ and 0.17 ± 0.22‰ for δD. As these values are below the total measurement error of $\delta^{18}O$ and δD values, and express an extreme scenario, here we use uncorrected data. We did not detect a memory effect with the funnel alone, which mimics the set up of the automated rain collector, where samples fall from the funnel into dry vials, so we also do not apply a memory effect to the samples from the automated precipitation collector.

All meteorological observations from the ARM Manus facility and are available through the ARM data directory (http://www.archive.arm.gov/discovery). Surface meteorological variables assessed here include 1 min resolution precipitation (RIMCO 7499, accuracy 1%), temperature and relative humidity (Vaisala HMP45 uncertainty ±0.57°C, 2.06%), atmospheric pressure (Vaisala PTB201A uncertainty 0.035 kPa), wind speed, and wind direction (R.M. Young Model 05106, uncertainty ±2%, 5°). Values of humidity (absolute and mixing ratios) used in this analysis are derived from site temperature and relative humidity. Here we report 5 min averages. In addition, we assess cloud base height measurements, derived from a Vaisala CL31 ceilometer (uncertainty ±1% or 5 m), which detects up to three cloud base heights to an altitude of 7600 m. Cloud base height data are the first detected cloud base height, in meters, reported in 5 min averages. We also use remotely sensed daily precipitation data for the broader region around Manus from the Tropical Rainfall Measuring Mission (TRMM) 3B42 product [*Kummerow et al.*, 1998], daily sea surface temperature (SST) from the Advanced Very High Resolution Radiometer (AVHRR) [*Reynolds et al.*, 2007], and the NOAA CPC MJO Index 4, which is located at 140°E, close to Manus Island [*Xue et al.*, 2002]. This index is calculated using extended empirical orthogonal function analysis of pentad 200 hPa velocity potential anomalies equatorward of 30° from 1979 to 2000 during ENSO neutral and ENSO weak November–April periods. Finally, we compare our in situ surface δD_v measurements to

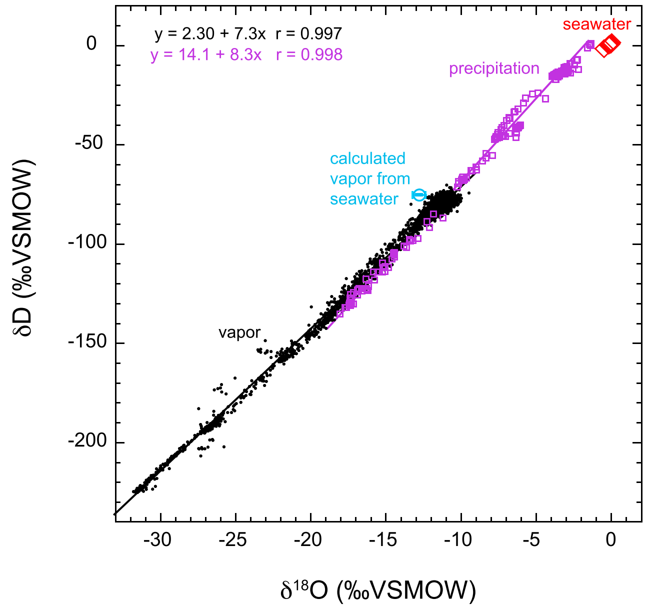

Figure 4. $\delta^{18}O$ and δD values of measured Manus vapor (black), precipitation (purple), and seawater (red). Blue circle represents calculated isotopic value of vapor derived from mean $\delta^{18}O_{sw}$, δD_{sw}, and daily SST accounting for kinetic fractionation with RH relative to SST and the *Gonfiantini* [1986] corrections for the kinetic effect. *R* values indicate correlation coefficient for $\delta^{18}O$ and δD.

satellite-derived, boundary layer δD_v observations from the Tropospheric Emission Spectrometer (TES, version 5) from September 2004 to December 2009 [*Worden et al.*, 2012]. We first calculated HDO/H_2O for each level and then averaged the data between 825 and 1000 hPa. Individual profiles from clear sky conditions (optical depth <0.1) and with more than 0.3 degrees of freedom were binned into monthly means on a 5°×5° grid. HDO data were corrected for the known 5.55‰ bias relative to the observations [*Worden et al.*, 2011]. We consider the cell nearest Manus (2°S, 145°E) in order to contextualize our near-surface vapor measurements.

3. Results

Over the 10 day period of measurement, mean 2 m air temperature was 27.3 ± 2.0°C and mean relative humidity (RH) was 83.8 ± 7.9% (1σ, based on 5 min averages). Both temperature and RH had a strong diurnal cycle (Figure 2). Mean wind speed was 1.4 ± 1.0 m/s and was predominantly westerly during the first 3 days of observation, becoming more southerly during the remaining 7 days. Precipitation was intermittent, with 10 rain events (7 of which were sampled for isotopic analysis) occurring over the 10 day period of observation. The precipitation rate was greatest on 28 April (>120 mm/h). Just to the west of Manus, a period of high precipitation occurred from 26 April to 29 April, at the beginning of the measurement period (Figure 3a). The 140°E MJO index also indicates a transition from regional convergence from 26 April to 28 April into a quiescent period that persisted through 8 May.

Over the period of measurement, mean $\delta^{18}O_v$ and δD_v values were −15.2 ± 5.4‰ and −108.2 ± 39.1‰ (1σ), respectively. We observed a 22.3‰ range in $\delta^{18}O_v$ and a 154.8‰ range in δD_v, from minimum values of −31.8 and −224.9‰ to maximum values of −9.5 and −71.0‰, respectively (Figure 4). The mean vapor deuterium excess value (dxs_v) was 13.8 ± 5.1‰ (1σ) (Figure 2). The lowest vapor isotope ratios and highest dxs_v values occurred during the first 3 days of measurement. $\delta^{18}O_v$ and δD_v values have a slope of 7.20 ± 0.02, similar to the global meteoric water line but with an intercept of 2.30 ± 0.35‰ (Figure 4). Mean $\delta^{18}O$ and δD values of precipitation (henceforth $\delta^{18}O_p$ and δD_p) were −7.2 ± 4.3‰ and −46.3 ± 35.4‰ (1σ), with values measured across individual events ranging from −17.7 to −1.4‰ for $\delta^{18}O_p$ and −132.0 to 1.0‰ for δD_p (Figure 4). Similar to vapor, the lowest precipitation isotope ratios occurred during the first 3 days of measurement but also during the 5 May rain event. The slope and intercept of the local meteoric water line from the precipitation data are 8.27 ± 0.08 and 14.09 ± 0.82‰, respectively. Temporally overlapping precipitation and vapor isotopic values were significantly correlated ($r = 0.94$, $N = 94$, $p < 0.001$ for δD). Mean isotope ratios from ocean sites ($\delta^{18}O_{sw}$ and δD_{sw} values) uninfluenced by runoff or freshwater films were 0.0 ± 0.1‰ (1σ) and 0.4 ± 0.5‰ (1σ), respectively (Data Set S1).

4. Discussion

4.1. Relationship Between δD_p, δD_v and Meteorological Variables

We observe a substantial transition from lower to higher δD_v and δD_p values over the observational period, coincident with a transition from a period of high regional precipitation associated with a mesoscale convective system into a regionally quiescent period (Figure 2). The observed δD_v values during the quiescent

Table 1. Correlation Coefficients (Spearman rank) of δD_v, δD_p, dxs_v, dxs_p, and Atmospheric Variables[a]

	δD_p (‰ VSMOW)	dxs_p (‰ VSMOW)	T (°C)	Precipitation (mm/hr)	RH air (%)	q (mmol/mol)	Wind (m/s)	Wind Direction	P (kPa)	Cloud Base (m)
δD_v (‰ VSMOW)	**0.94**	**0.49**	**0.67**	**−0.53**	**−0.53**	**0.72**	**0.19**	**−0.37**	**−0.21**	**−0.21**
dxs_v (‰ VSMOW)	**−0.40**	0.15	**−0.27**	**0.25**	**0.15**	**−0.46**	**0.08**	**0.15**	0.05	−0.03
δD_p (‰ VSMOW)		**0.47**	−0.08	0.06	−0.05	−0.19	−0.02	0.08	**−0.30**	0.12
dxs_p (‰ VSMOW)			**−0.34**	**0.40**	**0.50**	−0.21	0.04	0.09	**−0.57**	**−0.56**

[a]Bold values are significant at the 99% confidence level.

period are within the range of values reported by *Kurita* [2013] for the region (−90 to −80‰). The mean Manus δD_v value over the entire period of observation (−108.2 ± 39.1‰) is similar to the climatological mean boundary layer (825–1000 mbar) TES δD_v for April–May near Manus (TES April δD_v = −108 ± 29‰, TES May δD_v = −129 ± 20‰). The range of δD_v values observed at Manus is also comparable to δD_v values measured at 0.7°S, 73.2°E through an MJO event in November–December 2006, when 6 h resolution δD_v ranged from −165‰ to −80‰ [*Kurita et al.*, 2011]. During the quiescent period at Manus, measured δD_v approached calculated δD_v in equilibrium with mean δD_{sw} and the mean daily SST value of 29.6°C (Figure 4). After calculation of δD_v from δD_{sw}, kinetic fractionation was accounted for with relative humidity, calculated relative to mean SST over the campaign period, using the kinetic fractionation constants of 12.5 and 14.2‰ for δD and $\delta^{18}O$, respectively [*Gonfiantini*, 1986]. In the context of the MJO, the asymptotic approach to higher δD_v in equilibrium with surface conditions and lower dxs_v values demonstrates an approach toward steady state and surface recharge following active convective conditions [*Berkelhammer et al.*, 2012].

We find no significant evidence for a consistent amount effect on intraevent timescales; that is, considering 5 min δD_p and precipitation rate from all events pooled together. δD_p was most strongly correlated with δD_v and only weakly correlated with surface meteorological variables, including precipitation rate (Table 1). The high correlation coefficient between δD_p and δD_v may be due to surface vapor feeding the convective system via updrafts [*Kurita*, 2013] and/or rain vapor equilibration during rainfall. Assessing the relationship between surface meteorological variables and δD_v, we find strong, positive relationships between δD_v and water vapor concentration and δD_v and surface temperature (Table 1). There are also strong, negative correlations between δD_v and precipitation rate and δD_v and relative humidity. A negative correlation between δD_v and relative humidity was also observed in the Western Pacific in TES observations of midtroposphere water vapor associated with the region's intense convective activity [*Noone*, 2012]. The relationship between precipitation rate, water vapor concentration, and δD_v is a result of mixing, distillation, and evaporation processes (Figure 5): Higher water vapor content is coincident with vapor that has undergone less rainout, and the relationship between δD_v, temperature, and relative humidity suggests that warmer temperatures and lower relative humidity lead to higher δD_v via increased oceanic evaporation.

Wind speed and its influence on transport regime may also influence δD_v (and dxs_v) by altering the degree of turbulent mixing versus molecular diffusion of vapor [*Merlivat and Jouzel*, 1979; *Benetti et al.*, 2014]. However, similar to two other recent studies [*Steen-Larsen et al.*, 2014; *Benetti et al.*, 2015], we do not observe a relationship between δD_v and wind speed.

At Manus, the lack of a relationship between δD_v and wind speed may be partly due to the low variability in wind speed and relatively weak winds, which mainly fell within the smooth regime (<7 m/s). However, there is a stronger relationship between wind direction and δD_v, with lower δD_v coincident with more westerly winds. In conclusion, evidence suggests increased surface evaporation, via changes in surface temperature and relative humidity, leads to higher δD_v values and higher δD_p values. The influence of regional convection on δD_v is also strongly manifested in this dataset as lower δD_v values, despite the lack of anticorrelation between local rain rates and δD_p. In this way, our findings agree with those of *Moerman et al.* [2013], who observed a strong relationship between $\delta^{18}O_p$ and rainfall amount at timescales greater than 8 days but a weaker relationship on daily timescales. These studies strongly suggest that the tropical amount effect is driven by processes at the regional scale, as a function of shifting wind direction, differing moisture source, upstream convection, and transport of vapor that has undergone a different history of rainout.

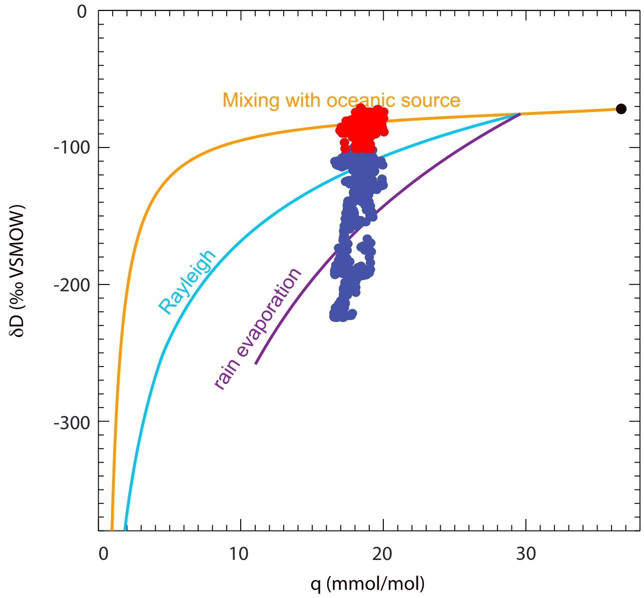

Figure 5. Mixing ratio (q, in mmol/mol) versus δD_v values. Blue dots represent 5 min averaged Manus data from period of strong regional convection and red dots represent 5 min averaged Manus data from subsequent quiescent period. Cyan line indicates vapor pathway following Rayleigh distillation, orange line indicates a mixing line between an upper atmosphere and oceanic source, and purple line indicate pathway representing re-evaporation of rain.

4.2. Role of Convective Processes in Determining dxs and δD

Despite the weak correlation between intraevent δD_p and meteorological variables (across all events), we find that intraevent precipitation deuterium excess (dxs_p) values are significantly correlated with surface relative humidity, temperature, precipitation, and sea level pressure, with higher dxs_p values occurring during periods of cooler temperatures, higher relative humidity, higher precipitation rates, and lower pressure. We also find that higher dxs_p values corresponded to lower cloud base altitudes. Although there is a strong correlation between δD_p and δD_v (Table 1), as well as $\delta^{18}O_p$ and $\delta^{18}O_v$ ($r = 0.98$, data in Table S2), we do not observe a significant correlation between dxs_v and dxs_p. Such a correlation would be predicted if moisture convergence, rather than kinetic processes (e.g., rain evaporation), dominates the amount effect within convective regions, as suggested in steady state simulations [*Moore et al.*, 2014]. The correlation coefficients between dxs_v and temperature, relative humidity, pressure, and cloud base height are also weaker relative to the correlation coefficients for dxs_p (Table 1). We also do not find a strong relationship between either dxs_p or dxs_v and wind speed, similar to other oceanic data sets, despite the theoretical basis for an influence of wind speed on dxs [*Steen-Larsen et al.*, 2014; *Benetti et al.*, 2015].

Monthly measurements of dxs_p have long been linked to surface climate variables in moisture source regions, especially relative humidity [*Merlivat and Jouzel*, 1979] and temperature [*Masson-Delmotte et al.*, 2005], as dxs_p values are largely set during evaporation. Dxs_v has also been shown to be conserved during transport from subtropical to high latitudes [*Bonne et al.*, 2015]. In this sense, higher temperatures and lower relative humidity at the site of evaporation and formation of the initial moisture source produce higher dxs_p values. Recent analyses suggest complexities in the interpretation of dxs, highlighting a more important role for relative humidity rather than temperature [*Lewis et al.*, 2013; *Pfahl and Sodemann*, 2014; *Steen-Larsen et al.*, 2014]. In the tropics, [*Risi et al.*, 2013] also hypothesized that on event timescales, rain re-evaporation and convection play stronger roles in controlling dxs_p values relative to evaporative surface conditions. Other work has also demonstrated that dxs can be an indicator of in-cloud processes, as well as subsidence [*Blossey et al.*, 2010; *Bolot et al.*, 2013]. At Manus, we find that the intraevent relationships between relative humidity, temperature, and dxs_p are the opposite sign of what is typically expected for the case of surface evaporation influences on longer timescales. That is, higher dxs_p coincides with lower surface air temperature and higher relative humidity, as well as increased precipitation, lower atmospheric pressure, and lower cloud base height. The direction of these relationships points to convective processes, namely, rain re-evaporation and subsidence (either at the larger scale or in association with downdrafts), as key drivers of dxs_p values [*Risi et al.*, 2013]. These results support the hypothesis that in this tropical, maritime region of high convective activity, dxs_p on intraevent timescales is a function of conditions during condensation, including post condensational exchange, rather than conditions only during evaporation. The highest measured dxs_v values in the Manus data set coincide with the lowest measured δD_v values and the lowest measured dxs_p values (Figure 2). As dxs_v and dxs_p should increase and decrease, respectively, due to rain evaporation [*Risi et al.*, 2013], these data support the hypothesis that dxs archives information about postcondensation processes as well as initial, surface evaporation, at least on short timescales.

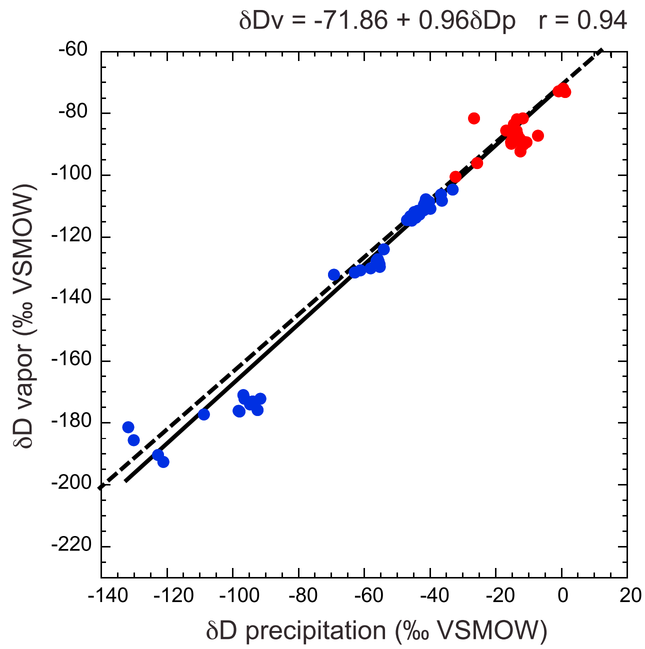

Figure 6. Manus δD_v versus δD_p values and linear regression equation. Blue dots represent 5 min Manus data from period of low δD_v, and red dots represent 5 min Manus data from subsequent quiescent period. Dashed black line represents hypothetical precipitation in equilibrium with vapor at mean surface air temperature (27.3°C).

A theoretical plot of the evolution of δD_v as a function of mixing ratio also shows that low δD_v values, coincident with high dxs_v, are related to subcloud rain evaporation [*Risi et al.*, 2008; *Kurita*, 2013; *Risi et al.*, 2013]. Figure 5 shows measured δD_v values versus the site mixing ratio, *q*, which provides a conceptual basis to interpret results. Following *Worden et al.* [2007] and *Noone* [2012], evolution lines are plotted showing an evaporation mixing curve between a dry end-member ($q = 0.9$ mmol/mol, $\delta = -360‰$) and vapor in equilibrium with an oceanic source at 26.8°C (300 K; black circle and orange line). The cyan line plots vapor that results from liquid precipitation following Rayleigh distillation that assumes an original vapor derived from an oceanic source with 80% relative humidity. The purple line denotes a similar evolution of a vapor mass following "super Rayleigh" distillation or a vapor mass that has experienced additional isotopic exchange due to rain evaporation, resulting in a steeper q-δD_v slope [*Noone*, 2012]. The location of the measured *q* and δD_v values in relation to these curves can thus guide interpretation of the dominant processes that determine δD_v in a particular data set. The lowest δD_v values measured at Manus fall on and below the rain evaporation line, pointing to rain evaporation as an influential process (which is supported by the lower dxs_p and higher dxs_v measurements) during the early part of the measurement period. The highest δD_v values, from the quiescent period, plot on or close to the ocean evaporation mixing line, supporting the observation that these δD_v values are primarily derived from ocean evaporation.

4.3. Relationship Between Intraevent δD_v and δD_p

The linear δD_v-δD_p relationship can reveal the signature of surface vapor in precipitation [*Kurita*, 2013]. At Manus, the relationship between all paired measurements of intraevent δD_v and δD_p has a slope of 0.96 ± 0.03, and an intercept of $-71.86 \pm 1.70‰$ (Figure 6). The calculated intercept for the Manus precipitation-vapor data set is within 1σ error of the intercept value of -73.07 for simulated tropical boundary layer δD_v and δD_p [*Moore et al.*, 2014] but is significantly higher than the intercept of -78.55 calculated using δD_v and δD_p from across the Pacific Ocean [*Kurita*, 2013]. The δD_v-δD_p slope at Manus is higher than a simulated tropical slope (0.88) [*Moore et al.*, 2014] and measured slope from the broader tropical Pacific region (0.72) [*Kurita,* 2013]. The higher slope at Manus relative to that of the open Pacific Ocean may indicate a greater proportion of stratiform rainfall at Manus during the measurement period. A greater ratio of stratiform to convective rainfall should produce a higher slope, as δD_p values of stratiform rainfall will be reduced relative to δD_p values in convective rainfall [*Kurita*, 2013].

An effective fractionation factor (R_p/R_v), calculated from simultaneous measurements of δD_v and δD_p, indicates whether precipitation is in equilibrium with boundary layer vapor at boundary layer temperatures or if other processes contribute to δD_p. Precipitation is not equilibrium with surface vapor if there is an isotopic offset between R_p/R_v and expected fractionation factors for given boundary layer temperatures. The effective fractionation factor can thus be diagnostic of equilibration between rain and boundary layer vapor or precipitation that formed in equilibrium with a vapor source unique from boundary layer vapor. In addition, when R_p/R_v exceeds the equilibrium fractionation factor for boundary layer temperatures, this may indicate additional fractionation due to rain evaporation.

At Manus, paired δD_v and δD_p values produce an average R_p/R_v value of 1.079 ± 0.007. Considered only as a function of temperature, 1.079 ± 0.007 reflects equilibrium condensation at boundary layer temperatures (~25°C) [*Majoube*, 1971] and agrees with simulated fractionation factors for precipitation derived from oceanic vapor [*Moore et al.*, 2014]. This recent simulation [*Moore et al.,* 2014] produced R_p/R_v values independent of precipitation rate, but we observe more variable R_p/R_v, often covarying with precipitation rate at the subevent scale, with R_p/R_v values ranging from 1.059 to 1.100 within individual rain events (Figure 7). However, combined uncertainty in δD_v and δD_p, expressed as a percentage of R_p/R_v, precludes interpretation of R_p/R_v for events with lower δD_v and δD_p, as the magnitude of uncertainty is equivalent or greater than variations in R_p/R_v (combined median uncertainty is 0.02). Hence, we simply conclude that within error, Manus R_p/R_v reflects condensation at boundary layer temperatures at these times. The exception is the 28 April rain event when the range of R_p/R_v (0.041, 1.059–1.100) exceeds combined uncertainty (0.01). This event occurred during the early period of enhanced regional convective activity and lower overall lower δD_v. During this rain event R_p/R_v decreased as precipitation rate increased.

There are several important implications that emerge from varying R_p/R_v during this precipitation event. Considering it first as only an indicator of temperature, R_p/R_v values imply condensation at temperatures ranging from 8.0°C ($\alpha = 1.100$) to 46.0°C ($\alpha = 1.059$). As average surface temperature ranged from 23.2°C to 31.0°C during the period of measurement, and the temperature was 20.0°C at the lifting condensation level (median cloud base height of 1300 m), other factors are clearly at play.

During the peak of the 28 April rain event, R_p/R_v was lower than expected for boundary layer temperatures. For events early in the field campaign, when evidence suggests that vapor was derived from a remote (westerly), and likely distilled source, vapor aloft may have had distinctly lower δD_v values than boundary layer vapor, which would be closer to equilibrium with seawater. In this case, δD_p and near-surface δD_v would not be in equilibrium; precipitation falling from higher in the atmosphere would have a δD_p value that would appear too negative relative to near-surface δD_v, producing lower R_p/R_v values.

R_p/R_v values exceeding the expected equilibrium fractionation factor for boundary layer temperatures, coincident with lower rain rates (e.g., at the beginning and end of the 28 April rain event), suggest either a greater influence of rain evaporation, imparting enhanced fractionation between vapor and precipitation, or precipitation in equilibrium with a vapor source independent from the measured boundary layer vapor. When dxs_p is low and R_p/R_v is high, such as at the beginning of the 28 April event, rain evaporation may be an important mechanism driving δD_p values. However, toward the end of the 28 April event, dxs_p is high when R_p/R_v is high, suggesting another mechanism at work. To produce higher R_p/R_v independent of increased kinetic fractionation due to rain evaporation, vapor aloft would have to have higher isotope ratios than near-surface vapor, leading to δD_p values that would appear too high relative to surface δD_v. Such a scenario may arise if vapor aloft has been recharged with surface vapor, perhaps from regions adjacent to the surface measurement site, while isotopically depleted, downdrafted vapor is present at the surface measurement site. Less variable R_p/R_v, independent of rain rate, when R_p/R_v remained within the boundaries of equilibrium fractionation factors for boundary layer temperatures, suggests a high degree of rain equilibration with boundary layer vapor (such as is associated with small rain drop populations as in the case of stratiform rain) or that precipitation was formed from vapor originally in the boundary layer.

4.4. The Amount Effect Within Individual Rain Events

Considering each individual rain event in the Manus data set, the relationship between precipitation rate and δD_p is variable. Thus, the negative correlation between precipitation intensity and isotope ratios (i.e., the amount effect) is manifested in some storms but not others: δD_p decreased simultaneously with increased precipitation rates and vice versa in the 28 April event, as well as in the 3 May and second 4 May events but not during the 30 April, first 4 May event, and 5 May event (Figure 7). In events with an amount effect, δD_p did not always remain low following peak rain rates but increased along with decreasing rain rate. This relationship argues against a condensation mechanism for the amount effect, as a progressive rainout of heavier isotopologues would lead to increasingly lower δD_p following peak rain rates. In these cases, advection of isotopically enriched vapor or updrafts of boundary layer vapor may play a role in driving the increase in δD_p toward the end of storms. During the 5 May event, the decrease in δD_p lagged the increase in rain rate and remained low following peak precipitation rates. However, dxs_p did not lag precipitation rate and increased prior to the decrease in δD_p, and dxs_p also led δD_p in the 28 April event. Greater investigation of this lag is warranted,

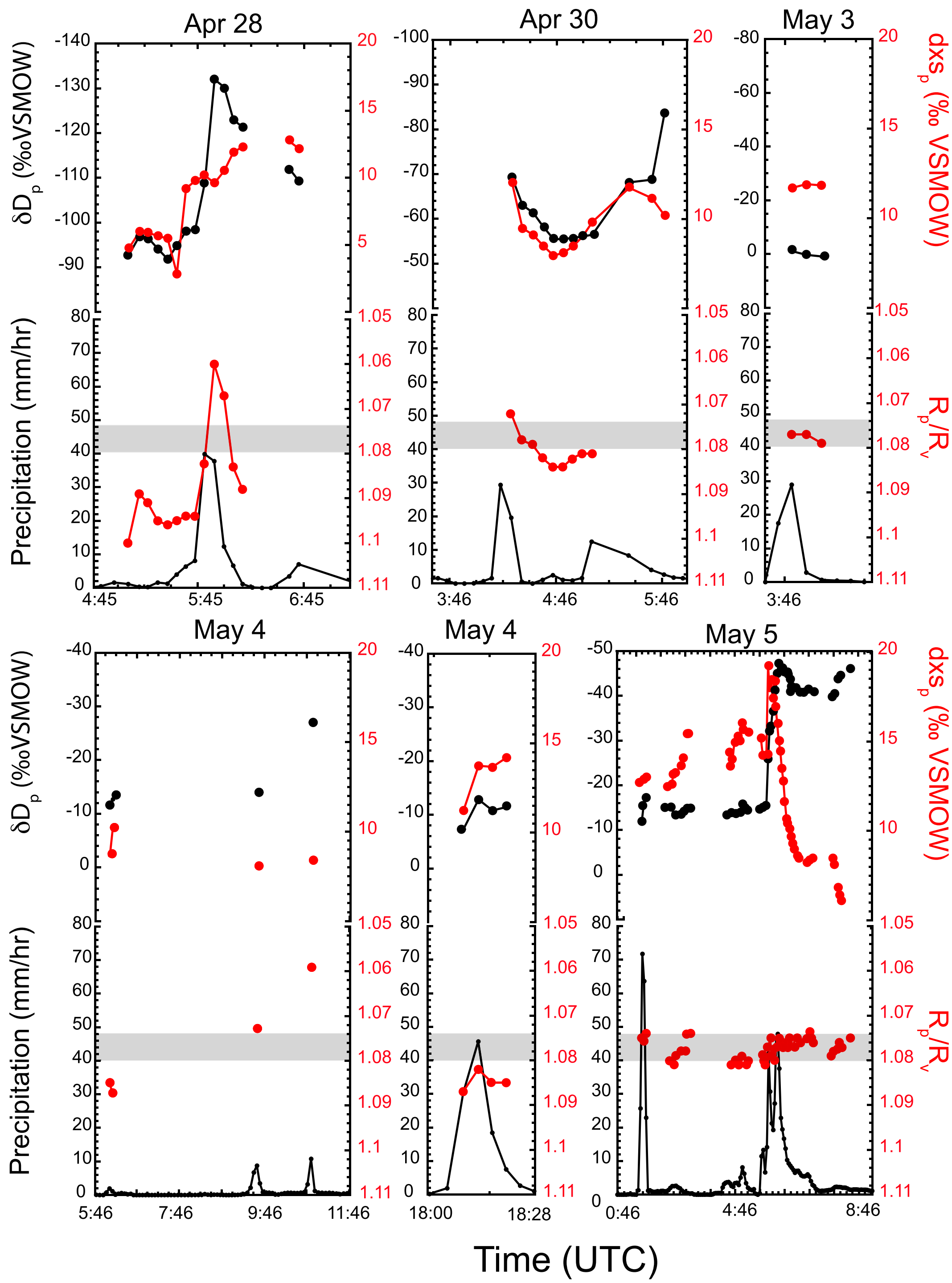

Figure 7. (top row) Precipitation rate (black) and R_p/R_v (red) calculated using isotope ratios in vapor and precipitation (red circles). (bottom row) δD_p (black) and dxs_p (red) through individual events. Gray shading denotes equilibrium fractionation factor range for average surface temperatures during events. Note that *y* axis is inverted for R_p/R_v and δD_p.

but one possible explanation is that rain evaporation, which would produce higher dxs_p values, may begin and be detectable in isotope ratios, prior to the influence of downdrafts on δD_p, which lower δD_p values as rain drops equilibrate with lower, upper atmosphere δD_v (relative to higher boundary layer δD_v). The manner in which these different processes aggregate to dominate the influence on monthly mean correlations between precipitation amount and isotope ratios in tropical areas (e.g., *Dansgaard* [1964]) remains unclear.

5. Conclusions

While there are several mechanisms that may explain the well-known negative correlation between precipitation amount and precipitation isotope ratios, we do not observe a consistent amount effect across seven precipitation events at Manus Island in the western equatorial Pacific Ocean. However, we do find evidence for differing degrees of atmospheric organization on precipitation isotope ratios on the synoptic (weekly) timescale. Large changes in δD_p and δD_v values over the 10 day period of measurement were related to a nearby mesoscale convective system, downwind advection of lower δD_v, and subsequently lower δD_p. During the more quiescent period that followed, δD_v approached values in equilibrium with local seawater and sea surface temperature and δD_p also increased. Thus, data from this measurement campaign supports the concept that an amount effect may result at synoptic scales from regional-scale convection, circulation, and downwind transport of depleted vapor [*Lawrence et al.*, 2004; *Kurita et al.*, 2009; *Kurita*, 2013], despite the variable relationship between precipitation amount and δD_p in individual precipitation events. However, the amount effect is apparent in some individual storms. Concurrent assessment of dxs_p, R_p/R_v, δD_p and precipitation amount can lend insight into the underlying controls on the drivers of the amount effect, or lack thereof, in individual events.

We find support for the role of postcondensational exchange on the isotopic ratio of precipitation and boundary layer vapor [*Risi et al.*, 2008]. Specifically, the lowest δD_v values measured, as well as coincident high dxs_v and low dxs_p values, indicate rain re-evaporation during the early part of the measurement campaign. However, as δD_p was not significantly correlated with rain rate during all precipitation events, rain evaporation and moisture recycling do not appear to produce a consistent amount effect in precipitation isotope ratios at intraevent timescales. Yet across all precipitation events, intraevent dxs_p values were correlated with surface temperature, precipitation rate, relative humidity, pressure, and cloud base height. Our data thus support a condensation control on dxs_p on the intraevent timescale, even though this parameter is more often interpreted as an indicator of conditions at the source of evaporation on longer timescales. Finally, we find that average R_p/R_v values suggest near equilibrium conditions due to either condensation or complete isotopic exchange at boundary layer temperatures. However, we also find more variable R_p/R_v during one rain event, with higher rain rates coincident with lower R_p/R_v and vice versa. This relationship suggests R_p/R_v may serve as an indicator of precipitation isotope ratios out of equilibrium with near-surface vapor isotope ratios, due to either enhanced rain evaporation or a vapor source distinct from the local boundary layer.

Apart from aiding in understanding modern convective processes, such metrics hold important implications for interpreting archives of past isotopic variability. For example, these results suggest that interpretation of dxs from low-latitude ice cores as reflective of evaporative conditions at the moisture source may be oversimplified; more investigation is required to understand how the signal recorded in dxs_p evolves across the differing timescales represented in various isotope archives. In addition, high temporal resolution proxies for the stable isotopic composition of precipitation, such as those that may reflect individual events [*Frappier et al.*, 2007], or intraseasonal variability [*Moerman et al.*, 2013, 2014] cannot necessarily be interpreted as proxies for local rain amount. Together, these findings offer observationally based interpretive guidance for proxies that reflect isotope ratios of precipitation in terms of precipitation characteristics in the tropics.

Acknowledgments
Funding sources for this work includes NSF-AGS-PF 1049664 to J.L.C., NSF ATM-0645291 to K.M.C., J.L.C., and D.N., as well as NNX08AR23G and 07-NEWS07-0020 to D.N. This research was supported by the Office of Biological and Environment Research of the U.S. Department of Energy as part of the Atmospheric Radiation Measurement Climate Research Facility. We would like to thank all ARM staff, Hymson Waffi, the Manus Weather Observers, John Glowacki, and Danthu Vu at Picarro for support in the field. Isotope data are available as supplementary files online. Tropospheric emissions spectrometer data available at http://tes.jpl.nasa.gov. ARM site data available at http://www.archive.arm.gov/discovery.

References

Araguas-Araguas, L., K. Froehlich, and K. Rozanski (2000), Deuterium and oxygen-18 isotope composition of precipitation and atmospheric moisture, *Hydrol. Processes*, *14*(8), 1341–1355.

Bailey, A., D. Toohey, and D. Noone (2013), Characterizing moisture exchange between the Hawaiian convective boundary layer and free troposphere using stable isotopes in water, *J. Geophys. Res. Atmos.*, *118*, 8208–8221, doi:10.1002/Jgrd.50639.

Bailey, A., D. Noone, M. Berkelhammer, H. C. Steen-Larsen, and P. Sato (2015a), The stability and calibration of water vapor isotope ratio measurements during long-term deployments, *Atmos. Meas. Tech.*, *8*, 5425–5466, doi:10.5194/amtd-8-5425-2015.

Bailey, A., J. Nusbaumer, and D. Noone (2015b), Precipitation efficiency derived from isotope ratios in water vapor distinguishes dynamical and microphysical influences on subtropical atmospheric constituents, *J. Geophys. Res. Atmos.*, *120*, 9119–9137, doi:10.1002/2015JD023403.

Benetti, M., G. Reverdin, C. Pierre, L. Merlivat, C. Risi, H. C. Steen-Larsen, and F. Vimeux (2014), Deuterium excess in marine water vapor: Dependency on relative humidity and surface wind speed during evaporation, *J. Geophys. Res. Atmos.*, *119*, 584–593, doi:10.1002/2013JD020535.

Benetti, M., G. Aloisi, G. Reverdin, C. Risi, and G. Sèze (2015), Importance of boundary layer mixing for the isotopic composition of surface vapor over the subtropical North Atlantic Ocean, *J. Geophys. Res. Atmos.*, *120*, 2190–2209, doi:10.1002/2014JD021947.

Berkelhammer, M., C. Risi, N. Kurita, and D. Noone (2012), The moisture source sequence of the Madden-Julian Oscillation as derived from satellite retrievals of HDO and H_2O, *J. Geophys. Res.*, *117*, D03106, doi:10.1029/2011JD016803.

Blossey, P. N., Z. Kuang, and D. M. Romps (2010), Isotopic composition of water in the tropical tropopause layer in cloud-resolving simulations of an idealized tropical circulation, *J. Geophys. Res.*, *115*, D24309, doi:10.1029/2010JD014554.

Bolot, M., B. Legras, and E. J. Moyer (2013), Modelling and interpreting the isotopic composition of water vapour in convective updrafts, *Atmos. Chem. Phys.*, *13*(16), 7903–7935.

Bonne, J. L., H. C. Steen-Larsen, C. Risi, M. Werner, H. Sodemann, J. L. Lacour, X. Fettweis, G. Cesana, M. Delmotte, and O. Cattani (2015), The summer 2012 Greenland heat wave: In situ and remote sensing observations of water vapor isotopic composition during an atmospheric river event, *J. Geophys. Res. Atmos.*, *120*, 2970–2989, doi:10.1002/2014JD022602.

Chiang, J. C. H. (2009), The tropics in paleoclimate, *Annu. Rev. Earth Planet. Sci.*, *37*, 263–297.

Coplen, T. B., P. J. Neiman, A. B. White, J. M. Landwehr, F. M. Ralph, and M. D. Dettinger (2008), Extreme changes in stable hydrogen isotopes and precipitation characteristics in a landfalling Pacific storm, *Geophys. Res. Lett.*, *35*, L21808, doi:10.1029/2008GL035481.

Dansgaard, W. (1964), Stable isotopes in precipitation, *Tellus*, *16*(4), 436–468.

Deng, L., S. A. McFarlane, and J. E. Flaherty (2013), Characteristics associated with the Madden–Julian oscillation at Manus Island, *J. Clim.*, *26*(10), 3342–3356.

Ellehoj, M., H. C. Steen-Larsen, S. J. Johnsen, and M. B. Madsen (2013), Ice-vapor equilibrium fractionation factor of hydrogen and oxygen isotopes: Experimental investigations and implications for stable water isotope studies, *Rapid Commun. Mass Spectrom.*, *27*(19), 2149–2158.

Frappier, A. B., D. Sahagian, S. J. Carpenter, L. A. Gonzalez, and B. R. Frappier (2007), Stalagmite stable isotope record of recent tropical cyclone events, *Geology*, *35*(2), 111–114.

Gonfiantini, R. (1986), Environmental isotopes in lake studies, in *Handbook of Environmental Isotope Geochemistry*, *The Terrestrial Environment*, vol. 2, edited by P. Fritz and J.-C. Fontes, pp. 113–168, Elsevier, Amsterdam.

Johnson, L. R., Z. D. Sharp, J. Galewsky, M. Strong, A. D. Van Pelt, F. Dong, and D. Noone (2011), Hydrogen isotope correction for laser instrument measurement bias at low water vapor concentration using conventional isotope analyses: Application to measurements from Mauna Loa Observatory, Hawaii, *Rapid Commun. Mass Spectrom.*, *25*(5), 608–616, doi:10.1002/rcm.4894.

Kummerow, C., W. Barnes, T. Kozu, J. Shiue, and J. Simpson (1998), The Tropical Rainfall Measuring Mission (TRMM) sensor package, *J. Atmos. Oceanic Technol.*, *15*(3), 809–817.

Kurita, N. (2013), Water isotopic variability in response to mesoscale convective system over the tropical ocean, *J. Geophys. Res. Atmos.*, *118*, 10,376–10,390, doi:10.1002/jgrd.50754.

Kurita, N., K. Ichiyanagi, J. Matsumoto, M. D. Yamanaka, and T. Ohata (2009), The relationship between the isotopic content of precipitation and the precipitation amount in tropical regions, *J. Geochem. Explor.*, *102*(3), 113–122, doi:10.1016/j.gexplo.2009.03.002.

Kurita, N., D. Noone, C. Risi, G. A. Schmidt, H. Yamada, and K. Yoneyama (2011), Intraseasonal isotopic variation associated with the Madden-Julian Oscillation, *J. Geophys. Res.*, *116*, D24101, doi:10.1029/2010JD015209.

Lawrence, J. R., S. D. Gedzelman, D. Dexheimer, H. K. Cho, G. D. Carrie, R. Gasparini, C. R. Anderson, K. P. Bowman, and M. I. Biggerstaff (2004), Stable isotopic composition of water vapor in the tropics, *J. Geophys. Res.*, *109*, D06115, doi:10.1029/2003JD004046.

Lee, J. E., I. Fung, D. J. DePaolo, and C. C. Henning (2007), Analysis of the global distribution of water isotopes using the NCAR atmospheric general circulation model, *J. Geophys. Res.*, *112*, D16306, doi:10.1029/2006JD007657.

Lewis, S. C., A. N. LeGrande, M. Kelley, and G. A. Schmidt (2013), Modeling insights into deuterium excess as an indicator of water vapor source conditions, *J. Geophys. Res. Atmos.*, *118*, 243–262, doi:10.1029/2012JD017804.

Madden, R. A., and P. R. Julian (1971), Detection of a 40–50 day oscillation in the zonal wind in the tropical Pacific, *J. Atmos. Sci.*, *28*(5), 702–708.

Majoube, M. (1971), Fractionnement en oxygene-18 et en deuterium entre l'eau et sa vapor, *J. Chem. Phys.*, *68*, 1423–1436.

Masson-Delmotte, V., J. Jouzel, A. Landais, M. Stievenard, S. J. Johnsen, J. W. C. White, M. Werner, A. Sveinbjornsdottir, and K. Fuhrer (2005), GRIP deuterium excess reveals rapid and orbital-scale changes in Greenland moisture origin, *Science*, *309*(5731), 118–121, doi:10.1126/Science.1108575.

Merlivat, L., and J. Jouzel (1979), Global climatic interpretation of the deuterium-oxygen-18 relationship for precipitation, *J. Geophys. Res.*, *84*(Nc8), 5029–5033, doi:10.1029/Jc084ic08p05029.

Miyake, Y., O. Matsubaya, and C. Nishihara (1968), An isotopic study on meteoric precipitation, *Pap. Meteorol. Geophys.*, *19*(2), 243–266.

Moerman, J. W., K. M. Cobb, J. F. Adkins, H. Sodemann, B. Clark, and A. A. Tuen (2013), Diurnal to interannual rainfall $\delta^{18}O$ variations in northern Borneo driven by regional hydrology, *Earth Planet. Sci. Lett.*, *369–370*, 108–119, doi:10.1016/j.epsl.2013.03.014.

Moerman, J. W., K. M. Cobb, J. W. Partin, A. N. Meckler, S. A. Carolin, J. F. Adkins, S. Lejau, J. Malang, B. Clark, and A. A. Tuen (2014), Transformation of ENSO-related rainwater to dripwater $\delta^{18}O$ variability by vadose water mixing, *Geophys. Res. Lett.*, *41*, 7907–7915, doi:10.1002/2014GL061696.

Moore, M., Z. Kuang, and P. N. Blossey (2014), A moisture budget perspective of the amount effect, *Geophys. Res. Lett.*, *41*, 1329–1335, doi:10.1002/2013gl058302.

Noone, D. (2012), Pairing measurements of the water vapor isotope ratio with humidity to deduce atmospheric moistening and dehydration in the tropical midtroposphere, *J. Clim.*, *25*(13), 4476–4494, doi:10.1175/jcli-d-11-00582.1.

Pfahl, S., and H. Sodemann (2014), What controls deuterium excess in global precipitation?, *Clim. Past*, *10*(2), 771–781, doi:10.5194/Cp-10-771-2014.

Reynolds, R. W., T. M. Smith, C. Liu, D. B. Chelton, K. S. Casey, and M. G. Schlax (2007), Daily high-resolution-blended analyses for sea surface temperature, *J. Clim.*, *20*(22), 5473–5496.

Riihimaki, L. D., and C. N. Long (2014), Spatial variability of surface irradiance measurements at the Manus ARM site, *J. Geophys. Res. Atmos.*, *119*, 5475–5491, doi:10.1002/2013JD021187.

Risi, C., S. Bony, and F. Vimeux (2008), Influence of convective processes on the isotopic composition (delta(18)O and delta D) of precipitation and water vapor in the tropics: 2. Physical interpretation of the amount effect, *J. Geophys. Res.*, *113,* D19306, doi:10.1029/2008jd009943.

Risi, C., A. Landais, R. Winkler, and F. Vimeux (2013), Can we determine what controls the spatio-temporal distribution of d-excess and ^{17}O-excess in precipitation using the LMDZ general circulation model?, *Clim. Past*, *9*(5), 2173–2193, doi:10.5194/Cp-9-2173-2013.

Rozanski, K., L. Araguas-Araguas, and R. Gonfiantini (1993), Isotopic patterns in modern global precipitation, in *Climate Change in Continental Isotopic Records*, edited by P. K. Swart, pp. 1–36, AGU, Washington, D. C.

Samuels-Crow, K. E., J. Galewsky, Z. D. Sharp, and K. J. Dennis (2014), Deuterium excess in subtropical free troposphere water vapor: Continuous measurements from the Chajnantor Plateau, northern Chile, *Geophys. Res. Lett.*, *41*, 8652–8659, doi:10.1002/2014GL062302.

Steen-Larsen, H. C., S. J. Johnsen, V. Masson-Delmotte, B. Stenni, C. Risi, H. Sodemann, D. Balslev-Clausen, T. Blunier, D. Dahl-Jensen, and M. Ellehøj (2013), Continuous monitoring of summer surface water vapor isotopic composition above the Greenland Ice Sheet, *Atmos. Chem. Phys.*, *13*(9), 4815–4828.

Steen-Larsen, H. C., A. E. Sveinbjörnsdottir, A. Peters, V. Masson-Delmotte, M. Guishard, G. Hsiao, J. Jouzel, D. Noone, J. Warren, and J. White (2014), Climatic controls on water vapor deuterium excess in the marine boundary layer of the North Atlantic based on 500 days of in situ, continuous measurements, *Atmos. Chem. Phys.*, *14*(15), 7741–7756.

Tremoy, G., F. Vimeux, S. Mayaki, I. Souley, O. Cattani, C. Risi, G. Favreau, and M. Oi (2012), A 1-year long delta O-18 record of water vapor in Niamey (Niger) reveals insightful atmospheric processes at different timescales, *Geophys. Res. Lett.*, *39*, L08805, doi:10.1029/2012GL051298.

van Geldern, R., and J. A. C. Barth (2012), Optimization of instrument setup and post-run corrections for oxygen and hydrogen stable isotope measurements of water by isotope ratio infrared spectroscopy (IRIS), *Limnol. Oceanogr. Methods*, *10*, 1024–1036.

Vimeux, F., R. Gallaire, S. Bony, G. Hoffmann, and J. C. H. Chiang (2005), What are the climate controls on delta D in precipitation in the Zongo Valley (Bolivia)?, Implications for the Illimani ice core interpretation, *Earth Planet. Sci. Lett.*, *240*(2), 205–220, doi:10.1016/J.Epsl.2005.09.031.

Vuille, M., R. S. Bradley, M. Werner, R. Healy, and F. Keimig (2003), Modeling delta O-18 in precipitation over the tropical Americas: 1. Interannual variability and climatic controls, *J. Geophys. Res.*, *108*(D6), 4174, doi:10.1029/2001JD002038.

Worden, J., D. Noone, K. Bowman, and T. E. Spect (2007), Importance of rain evaporation and continental convection in the tropical water cycle, *Nature*, *445*(7127), 528–532.

Worden, J., S. Kulawik, C. Frankenberg, V. Payne, K. Bowman, K. Cady-Peirara, K. Wecht, J. E. Lee, and D. Noone (2012), Profiles of CH_4, HDO, H_2O, and N_2O with improved lower tropospheric vertical resolution from Aura TES radiances, *Atmos. Meas. Tech.*, *5*(2), 397–411, doi:10.5194/amt-5-397-2012.

Worden, J., D. Noone, J. Galewsky, A. Bailey, K. Bowman, D. Brown, J. Hurley, S. Kulawik, J. Lee, and M. Strong (2011), Estimate of bias in Aura TES HDO/H2O profiles from comparison of TES and in situ HDO/H2O measurements at the Mauna Loa observatory, *Atmos Chem. Phys.*, *11*(9), 4491–4503, doi:10.5194/Acp-11-4491-2011.

Xue, Y., W. Higgins, and V. Kousky (2002), Influences of the Madden Julian Oscillation on Temperature and Precipitation in North America during ENSO-Neutral and Weak ENSO winters, *A Workshop on Prospects for Improved Forecasts of Weather and Short-term Climate Variability on Subseasonal (2 Week to 2 month) Time Scales*, edited by S. Schubert et al., pp. 116–119. NASA/Goddard Space Flight Center.

Yoshimura, K., M. Kanamitsu, D. Noone, and T. Oki (2008), Historical isotope simulation using reanalysis atmospheric data, *J. Geophys. Res.*, *113*, D19108, doi:10.1029/2008JD010074.

Yoshimura, K., M. Kanamitsu, and M. Dettinger (2010), Regional downscaling for stable water isotopes: A case study of an atmospheric river event, *J. Geophys. Res.*, *115*, D18114, doi:10.1029/2010JD014032.